




Effect of citral partitioning on structural and mechanical properties of lipid membranes

Deepashri Saraf^{1,a}, Sudha Porte^{1,2,b}, and Durba Sengupta^{1,2,c} 

¹ CSIR-National Chemical Laboratory, Dr. Homi Bhabha Road, Pune, Maharashtra 411008, India

² Academy of Scientific and Innovative Research (AcSIR), Ghaziabad, Uttar Pradesh 201002, India

Received 14 December 2023 / Accepted 5 March 2024

© The Author(s), under exclusive licence to EDP Sciences, Springer-Verlag GmbH Germany, part of Springer Nature 2024

Abstract Delineating the interactions of cellular metabolites with lipid membranes and their effects on membrane physical and mechanical properties constitutes a key step for comprehensively understanding their biological function. The plant metabolite—citral is widely used in biotechnological and cosmeceutical processes, but significant gaps remain in our understanding of how it affects cellular membranes that it interacts with. In this study, we unravel the molecular mechanisms underlying the interactions of citral with compositionally distinct model membranes using atomistic molecular dynamics simulations. Specifically, we investigate two distinct membrane compositions: the neutral phosphatidylcholine-phosphatidylethanolamine (DOPC:DOPE) bilayer, representing mammalian cell membranes and the anionic phosphatidylcholine-phosphatidylglycerol (DOPC:DOPG) bilayer, mimicking bacterial cell membranes. Our simulations reveal that citral molecules readily partition into both membranes without distinct composition-dependent effects. Monomeric citral molecules localize mainly at the interface of the acyl chain region of the lipids, and a few translocation events are sampled in the simulations. Interestingly, we observe small differences in lipid fluidity although the citral molecules significantly influence the rigidity of lipid bilayers, and a higher bending modulus was observed in DOPC:DOPE lipid bilayers compared to DOPC:DOPG bilayers. Further, citral partitioning induces an increased tendency for lipid demixing in DOPC:DOPE membranes, as evidenced by the decreased values of the Shannon entropy. Our work is an important step to elucidate the molecular processes that underlie the differential impact of cell metabolites on compositionally distinct lipid membranes.

1 Introduction

The semi-permeable cell membrane acts as a protective barrier from the external environment, and plays a vital role in biological processes such as transport, cell signaling and cell–cell adhesion [1–4]. The membrane bilayer consists of a complex composition of diverse lipids and proteins [5] that gives rise to heterogeneous lamellar structure with lateral and depth-dependent anisotropy [6–10]. Further, the structural and mechanical properties of lipid bilayers are sensitive to the specific type and composition of the lipids that differ across cell types and organisms [11, 12]. In fact, small changes to membrane fluidity and acyl chain order parameters may alter membrane protein function, and therefore, are usually regulated by cells [13, 14]. Differential order within the membrane has been shown to result in lipid demixing and the formation of lipid micro/nanodomains, which have been attributed different functional roles [15]. Mechanical properties such as bending rigidity are not only critical for cell function such as endo- and exo-cytosis and trafficking but also for overall membrane integrity [14, 16]. Since the lipid bilayer selectively allows small molecules to partition or permeate through based on their physico-chemical properties [17–20], cell metabolites and xenobiotics (non-host metabolites) differentially interact with these lipid membranes. Importantly, the interactions of metabolites may alter the lipid physical properties, leading to changes in membrane structure and mechanics that can have an important impact on biological processes, such as cell signaling, ion transport, and membrane fusion [14]. In general, the partitioning of small molecule metabolites has been well studied [19–22]

^a e-mail: d.saraf@ncl.res.in

^b e-mail: s.porte@ncl.res.in

^c e-mail: d.sengupta@ncl.res.in (corresponding author)

although their exact localization within the membrane and how they modulate membrane properties are relatively less clear.

Secondary metabolites derived from plants have long been used as food supplements and in traditional medicinal systems for their various health benefits [23]. Terpenes are a class of secondary plant metabolites that are widely distributed in nature, particularly in essential oils derived from plants. They have been reported to exhibit various biological activities, such as antimicrobial [24], anticancer [25, 26], and anti-inflammatory effects [27]. Monoterpenes are a subgroup of terpenes, consisting of two isoprene units, which can be arranged in different configurations to form different monoterpenes. Spectroscopy studies of monoterpenes and lipid membranes have shown that the hydrophobicity and structure of the monoterpenes play a crucial role in their interactions with lipid membranes [28]. Among the monoterpenes, citral is an unsaturated aldehyde having stereoisomers citral-A and citral-B with the molecular formula $C_{10}H_{16}O$. It is widely used in the food and perfumery industries as an aroma compound. Its bioactive properties, such as its anti-inflammatory [29], anti-tumor [30, 31], and anti-bacterial [32] activities, make it a potential candidate for drug development, although it is prone to drug interactions and oxidation, which limits its use [33]. Interactions of citral molecules with lipid membranes have been reported to lead to membrane disruption, and suggested to be a key step in its antimicrobial activity [34]. Understanding the chemical and biological properties of citral and its interactions with the cell membrane is crucial in maximizing its therapeutic applications.

Classical molecular dynamics (MD) simulations are a powerful tool to study membrane and small molecule metabolite dynamics at a molecular resolution [22, 35]. Molecular dynamics simulations of metabolite permeation into lipid bilayers can be cross-validated against experiments by comparing macroscopic observables, such as partitioning, membrane thickness and fluidity [17]. In addition, simulations can reveal a level of detail that is frequently difficult to obtain experimentally, thus offering an additional perspective to experiments. Molecular dynamics simulations have been shown to reproduce physico-chemical characteristics of model membranes as well as membranes of more complex compositions [9, 19, 36] and have been successfully used to study membrane structural and mechanistic properties [37–41], curvature [42] and passive transport across membranes [17, 43].

In particular, molecular dynamics simulations have been used to study metabolites and xenobiotics that have been shown to exert antimicrobial and anti-hemolytic activity by partitioning into and subsequently perturbing the lipid bilayer considerably. For instance, the differential partitioning of antimicrobial molecules, withaferin-A and withanone across 1-Palmitoyl-2-oleoylphosphatidylcholine (POPC) model membrane has been studied using atomistic simulations and validated with the experimental results [44]. An anti-bacterial agent, chlorhexidine has been shown to be responsible for the thinning of 1,2-dimyristoyl-sn-glycero-3-phosphocholine (DMPC) bilayer using classical molecular dynamics simulations [45]. Further, the partitioning and translocation of bacterial quorum sensing modulators in pure 1,2-dioleoyl-sn-glycero-3-phosphocholine (DOPC) and mixed 1-palmitoyl-2-oleoyl-phosphatidylethanolamine (POPE) and 1-palmitoyl-2-oleoyl-sn-glycero-3-phosphatidylglycerol (POPG) membranes have been rigorously analyzed [46]. The monoterpenes, thymol and geraniol were shown to cause pronounced melting point depression and phase segregation in DMPC lipid bilayers depending on the hydration conditions [47]. A recent molecular dynamics study on plant terpenoids, leubethanol, abietic acid, and sclareol suggests that their permeability is greater for plant-like membrane compositions as compared to animal-like membrane models [48]. To the best of our knowledge, there are no such studies available particularly on citral molecules, despite their biotechnological applications.

In this study, we use all-atom classical molecular dynamics simulations to investigate the mechanistic aspects of citral–membrane interactions. Our main focus is on the citral-A isomer (referred to as “citral”). We analyze two distinct bilayer membranes representing mammalian and bacterial membranes, by varying the lipid compositions. We consider both, citral monomers and clusters and probe their partitioning and impact on the physico-chemical properties of the lipid bilayer, such as acyl chain order parameter, average lipid area, bilayer thickness, and bending modulus. We further explore how citral molecules influence the segregation of different lipid species using the Shannon entropy formalism. Our work provides valuable insights into the underlying mechanisms of monoterpenes, offering potential applications in the development of novel drugs and drug delivery systems.

2 Computational methodology

All-atom molecular dynamics simulations were performed of citral and lipid bilayers with the CHARMM36 force-field [49] and GROMACS simulation package version 2018 [50]. The structural parameters for citral-A molecule were obtained from CGenFF suite [51, 52] and previously validated [53]. Figure 1a depicts the chemical structure of citral. Two bilayer compositions were considered (i) dioleoyl-sn-glycero-3-phosphocholine (DOPC) and dioleoyl-sn-glycero-3-phosphoethanolamine (DOPE) lipids with a ratio of 70:30, i.e., $DOPC_{0.7}DOPE_{0.3}$ and (ii) DOPC and dioleoyl-sn-glycero-3-phosphoglycerol (DOPG) with the ratio of 70:30, i.e., $DOPC_{0.7}DOPG_{0.3}$. In chemical terms, DOPC, DOPE, and DOPG are phospholipids with a glycerol backbone and two oleic acid chains and choline, ethanolamine and glycerol headgroups, respectively (see Fig. 1a).

The bilayers were modeled using the CHARMM-GUI module [54] with dimensions of 18×18 nm. They consisted of 960 lipid molecules and were further solvated using TIP3P water model [55]. In case of DOPC_{0.7}DOPG_{0.3} membrane, adequate numbers of K⁺ and Cl⁻ ions were added in the simulation box to attain the charge neutrality. Following a common convention, the lipid bilayers were arranged in a flat layer parallel to the XY-plane, with the Z-axis perpendicular to the membrane.

In the citral monomer simulations, the starting arrangement consisted of 30 randomly arranged citral molecules that were placed in the water layer away from the membrane. All simulations were performed in three replicate sets. For the citral cluster simulations, we first performed simulations in aqueous solvent at multiple concentrations by varying number ratios between 1:555 and 1:75. Two of the clusters that were formed (ratios 1:555 and 1:75) were then placed in the pre-equilibrated membrane simulation box in the surrounding water layer. The molecules were simulated in water for 200 ns and membrane simulations were performed for 1 μs.

An integration time step of 2 fs was used. The distribution of temperature was ensured with the V-rescale thermostat at temperature 300 K and coupling constant of 0.1 ps [56, 57]. Isotropic pressure coupling was used for citral self-assemblies in water, whereas citral–membrane interactions were studied with the semi-isotropic pressure coupling. In both cases, the Parrinello–Rahman barostat scheme was used, with a reference pressure of 1.0 bar, a coupling constant of 2 ps and a compressibility of $4.5 \times 10^{-5} \text{ bar}^{-1}$ [58]. The LINCS algorithm was used for bond constraints [59].

2.1 Analysis

The molecular dynamics trajectories were analyzed with in-house scripts and GROMACS utilities. The snapshots of the different systems were rendered with VMD [60]. Membrane thickness and area per lipid were calculated using the utility, FATSLiM [61].

Aggregate properties: The propensity of clustering in the aggregates was analyzed using standard GROMACS utilities. The aggregation number was calculated as number of clusters (n_{clust}) found at each time step normalized by total number of molecules in the simulation ($N_{\text{molecules}}$) as a function of time for each composition ($n_{\text{clust}}/N_{\text{molecules}}$).

Shannon entropy: The entropy of mixing for the DOPC_{0.7}DOPE_{0.3} and DOPC_{0.7}DOPG_{0.3} binary mixtures was calculated based on Shannon's entropy that in the mean field approximation is given by,

$$S = - \sum_x p(x) \log p(x), \quad (1)$$

where $p(x)$ is the probability of system being in a state x .

For the discrete systems that we are using, it would be imperative to calculate the probability of finding two different lipids (DOPC/DOPE or DOPC/DOPG) next to each other. Hence, we use the improvement proposed by Camesasca et al. [62] that is to subdivide the space into N regions, and then evaluate the Shannon entropy of each region i as,

$$S_i = - \sum_x p_i(x) \log p_i(x), \quad (2)$$

where $p_i(x)$ is the number of lipids of type x in region i divided by the total number of lipids in that region. The entropy of mixing of the whole system is then estimated as the average of the entropies over all sub-regions.

$$S = - \frac{1}{N} \sum_i \sum_x p_i(x) \log p_i(x). \quad (3)$$

For a binary system in 2D, the values range between 0 and 0.69. Based on the size of the lipids, it was found that the grid size, $3 \leq N \leq 5$, produced quantitatively consistent results. This formalism was used in our earlier work on demixing in the isomeric mixtures of citral self-assemblies [53] and can be referred to for more details.

Membrane bending modulus: The mechanical properties of the membranes were calculated using the bending modulus. Membrane bending modulus calculation was proposed by W. Helfrich based on continuum mechanical theory in early '70s [63]. Our work uses a method developed in the references [64, 65] based on the same formalism. In this method, the bending modulus ($S(q)$) is determined from a Fourier analysis of the height fluctuations (h) in the membrane of area (A), which results in the following,

$$S(q) = \langle |h(q)|^2 A \rangle, \quad (4)$$

$$S(q) = \frac{k_B T}{\kappa q^4 + \gamma q^2}, \quad (5)$$

where κ is the bending rigidity, γ is the membrane tension, k_B is the Boltzmann constant, T the temperature and q the wave number.

3 Results

To investigate the effect of citral on the model membrane bilayers, we considered both monomeric citral molecules dispersed in water as well as citral clusters. Atomistic molecular dynamics simulations were performed at a microsecond timescale and we observed that the citral molecules first diffused in water as individual monomers or clusters and subsequently partitioned into the membranes. The chemical structures and representative snapshots of the simulation setups are shown in Fig. 1. Overall, we observed that the citral molecules have a strong affinity for both bilayer membranes. We analyzed the localization of the citral molecules and their effects on the lipid membranes.

3.1 Partitioning of citral molecules into the membrane

In the first step, we considered the monomeric citral molecules in the water layer and observed that the molecules that were in the close vicinity to the bilayer had a high probability to partition into it. The molecules that were further away from the membrane diffused in water before partitioning into the membrane. Interestingly, despite their amphiphilic nature, the citral molecules did not aggregate either before or after partitioning into the membrane. It was observed that most of the citral molecules partitioned into the membrane within 500 ns of the simulation and remained bound to the membrane during the timescales of the simulations. The time evolution of their membrane partition is shown in Fig. 1b.

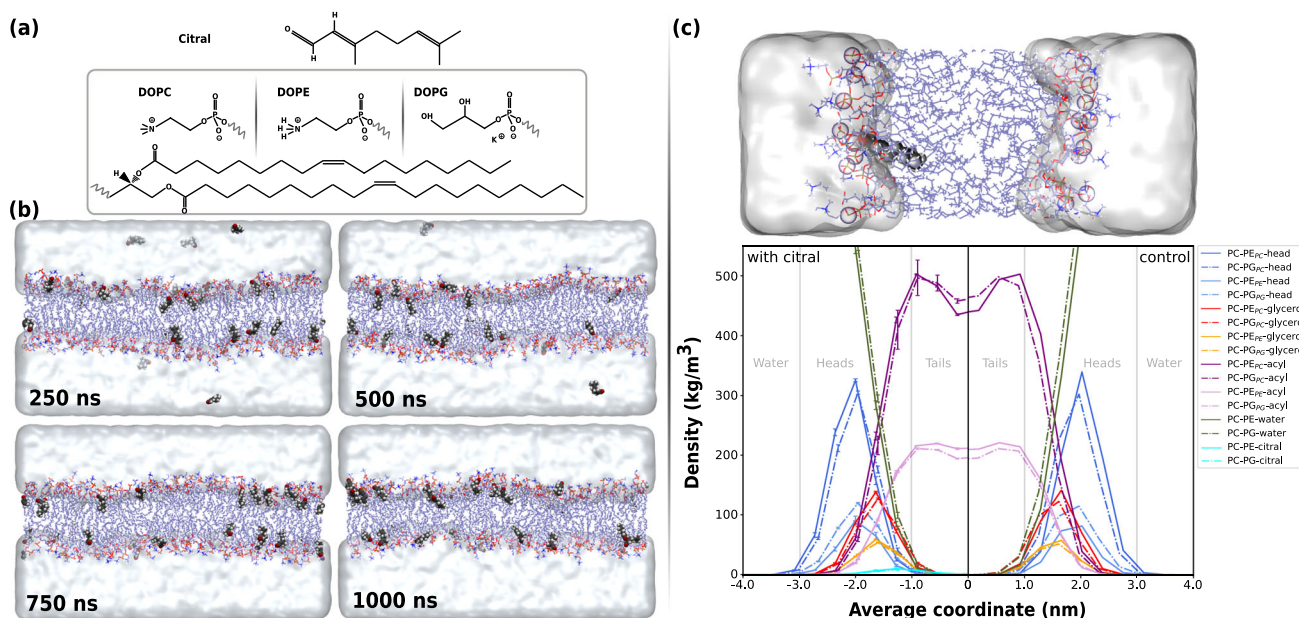


Fig. 1 **a** Chemical structures of citral, DOPC, DOPE, and DOPG. **b** A time series of representative snapshots of citral molecules in DOPC_{0.7}–DOPE_{0.3} membranes. Citral molecules are depicted in spherical (van der Waal) representation with carbon atoms in gray, hydrogen atoms in silver, and oxygen atoms in red colored beads. The lipids are shown with line representation with purple color depicting the carbon atoms, red for the oxygen atoms and blue for the nitrogen atoms. Lipid headgroups are represented by the phosphorus atoms as unfilled purple beads. The surrounding water is rendered in white surface representation. The color scheme is maintained throughout the article. **c** Density profile of different constituents of the lipid bilayers as a function of distance from the bilayer center in presence (left panel) and absence (right panel) of citral molecules for DOPC_{0.7}DOPE_{0.3} and DOPC_{0.7}DOPG_{0.3} membranes. The standard deviations obtained from averaging the data on replicate simulation sets are shown as whiskers for the case of citral–membrane system. The structure of membrane aligned with the densities is shown in the top panel

To analyze the localization of the citral molecules in the membrane, we calculated the mass density profile of the membrane, decomposed into the constituent chemical moieties such as lipid headgroups, glycerol, acyl chains, water, and citral molecules (shown in Fig. 1c). For a direct comparison, only one of the membrane leaflets is shown and the plot is subdivided into two panels: the left panel depicts the membrane with citral molecules and the right panel depicts the same bilayer membrane in the absence of the citral molecules. Further, the solid lines represent the DOPC_{0.7}DOPE_{0.3} membrane and the dashed lines represent the DOPC_{0.7}DOPG_{0.3} membrane. The three distinct domains, the water, headgroup, and tail regions of the membrane are easily discerned and marked on the figure. The interface region forming the boundary between the lipid headgroups (depicted as shades of blue in the plot) and water (green) ranges from 2.0 to 3 nm from the bilayer center. The glycerol groups (depicted in yellow and red) form the interface to the acyl chains of the phospholipids (pink, purple) that extends to about 1–3 nm from the bilayer core. The average location of the citral molecules (cyan) is in the region of the boundary between the glycerol group and acyl chains. Interestingly, the average position of citral molecules is the same in both membrane compositions, despite marginal differences in the density profile for the other moieties. We were unable to distinguish any significant differences between the density profile in the presence and absence of the citral molecules, suggesting that citral molecules do not extensively perturb or remodel the membrane at these concentrations.

The orientational flexibility of the citral molecules within the membrane is limited due to the complex electrostatic environment of the membrane. We analyzed the molecular orientation, calculated as the angle between the main molecular axis and the membrane normal, and plotted the kernel density distribution with respect to the membrane normal (z) over the simulation time (see Fig. S1). We observed that it ranges around 30° or 150°, depending on the membrane leaflet it is present in.

3.2 Translocation of citral molecules through the membrane

During the course of the trajectory, we observed a few transbilayer diffusion events in which a citral molecule diffused from one membrane leaflet to the other. Representative snapshots detailing the translocation of a single citral molecule is given in Fig. 2. While “flip-flopping” from one leaflet to the other, the citral molecules reoriented the oxygen atoms such that it faces the headgroups of the lipids. The molecule quickly moved toward the other leaflet by reorienting its head, i.e., the oxygen atom toward the headgroups of the opposing leaflet. No bound water molecules were observed during the transbilayer diffusion, i.e., the hydroxyl group was desolvated. Further, we re-analyzed the orientation of the citral molecules within the membrane and observed that the molecules adopted an orientation that allowed the doubly bonded oxygen to point outwards toward the water layer during a large fraction of the time of the translocation event (see Fig. S1).

The position of all citral molecules along the membrane normal highlighting the translocation events is shown in Fig. S2 and S3 for DOPC_{0.7}–DOPE_{0.3} and DOPC_{0.7}–DOPG_{0.3} membranes, respectively. It can be seen that about half of the citral molecules translocate between the two bilayer leaflets while the rest remain localized to the same leaflet. Despite the transbilayer diffusion events, an asymmetry is maintained in the number of citral molecules bound to each leaflet. Each of the translocation events occurs within a few nanoseconds and an average translocation time was estimated to be 25–180 ns. A simple in-house script was used to count the translocation

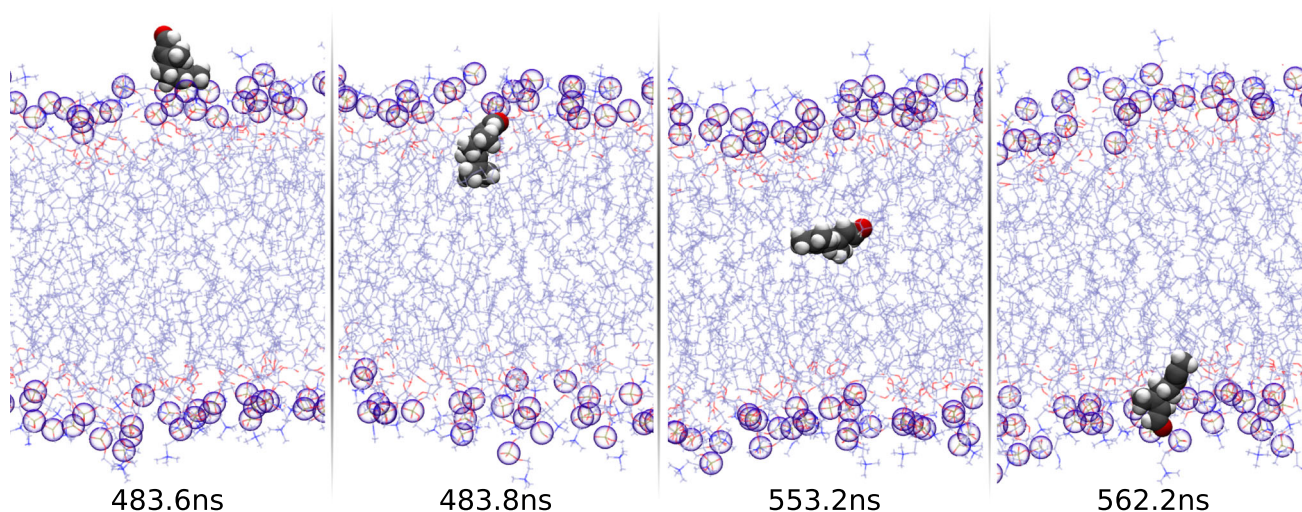


Fig. 2 Translocation of a citral molecule across DOPC_{0.7}–DOPE_{0.3} membrane in a time-series representation

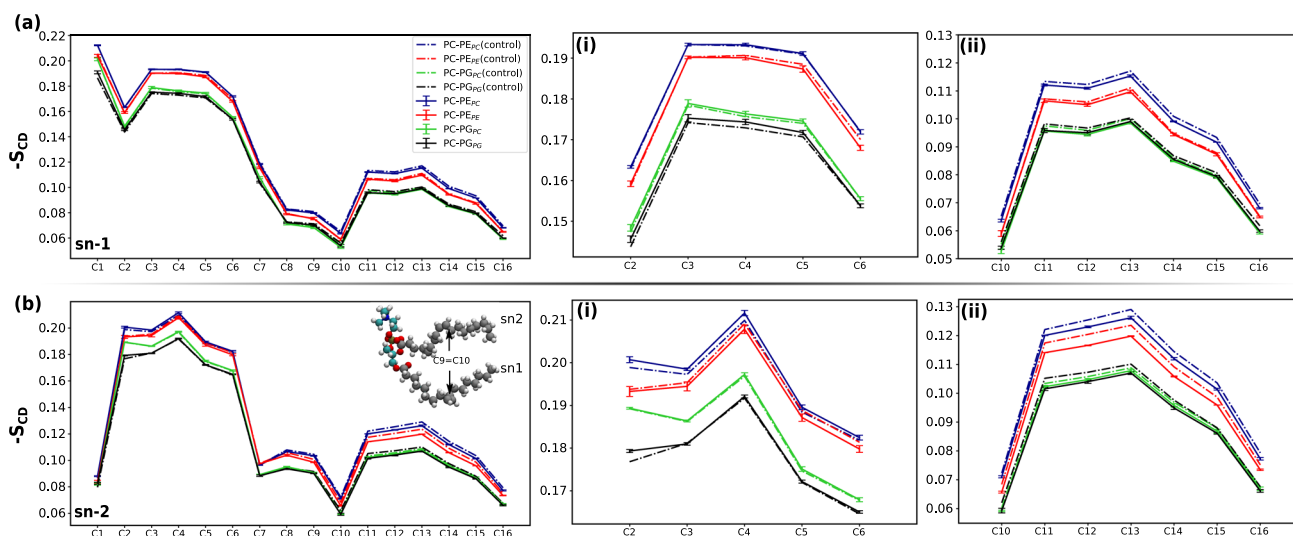


Fig. 3 The lipid tail order parameter ($-S_{CD}$) as a function of the carbon number in **a** sn-1 chain and **b** sn-2 chain of $\text{DOPC}_{0.7}\text{DOPE}_{0.3}$ and $\text{DOPC}_{0.7}\text{DOPG}_{0.3}$ lipid membranes in presence and absence of citral molecules. For both the figures, the zoom-in plots of certain sections are shown in subfigures (i, ii) alongside (a, b). Figure legends are shown in the inset of (a), whereas the inset of (b) shows the molecular representation of DOPC along with its sn-1 and sn-2 chains and the double bond between C9 and C10 sites for reference. The standard deviations obtained from averaging the data on replicate simulation sets are shown as whiskers for the case of citral–membrane system

events and time-frames from the plots in Figs. S2 and S3. The average translocation rate was then estimated to be $6.3 \times 10^{-7} \text{ s}^{-1}$ in $\text{DOPC}_{0.7}\text{DOPE}_{0.3}$ and $7.6 \times 10^{-7} \text{ s}^{-1}$ in $\text{DOPC}_{0.7}\text{DOPG}_{0.3}$ membranes. However, longer sampling is required for quantitative estimates due to the limited sampling.

3.3 Citral modulates the membrane fluidity or order

To analyze the membrane fluidity changes upon citral adsorption, the acyl chain order parameters ($-S_{CD}$) of the membranes are shown in Fig. 5. The order parameter values of the membranes follow a similar trend as previously reported in simulations [66, 67]. For a better comparison, the sn-1 and sn-2 chains are plotted separately since the order parameters differ due to the different alignment of the acyl chains. Overall, the $\text{DOPC}_{0.7}\text{DOPE}_{0.3}$ membranes have a higher order than the $\text{DOPC}_{0.7}\text{DOPG}_{0.3}$ membranes. Surprisingly, the differences in the acyl chain order parameters in the presence or absence of citral are marginal toward the glycerol-end of the acyl chain, in the proximity of the citral localization. However, toward the bilayer core the membrane fluidity increases in the presence of the citrals and the order parameters of the terminal carbon atoms differs significantly. From the results, it is clear that the citral molecules modulate the fluidity or packing of the lipid tails of both the lipid bilayers, upon partitioning into the membrane.

In conjunction to the membrane fluidity changes, membrane volume and area per lipid are often modulated. The average thickness and area per lipid was calculated for both the bilayers and shown in Fig. S4a, b, respectively. From Fig. S4, it can be seen that the $\text{DOPC}_{0.7}\text{DOPE}_{0.3}$ bilayer has higher average thickness of $\sim 3\%$ than the $\text{DOPC}_{0.7}\text{DOPG}_{0.3}$ bilayer. Partitioning of citral molecules within the membranes reduces the average membrane thickness for both the membranes. Further, the average area per lipid of DOPC, DOPE and DOPG lipids is modulated and a small increase is observed in the presence of the citral molecules.

3.4 Citral partitioning alters the bending modulus of the membrane

Large bilayer fluctuations and undulations were visible during the course of the simulations, as also evident in the time-series snapshots (see Fig. 1b). However, no persistent curvature could be discerned due to the diffusion of the citral molecules. To quantify the differences in these fluctuations, we calculated the undulation spectra of the bilayer and fitted the low q (wave number) regime to q^{-4} . Figure 4 shows the undulation spectra and the bending moduli, κ calculated for the $\text{DOPC}_{0.7}\text{DOPE}_{0.3}$ and $\text{DOPC}_{0.7}\text{DOPG}_{0.3}$ lipid membranes with and without citral molecules. The control simulations show that $\text{DOPC}_{0.7}\text{DOPG}_{0.3}$ bilayer has a marginally lower bending modulus than that of the $\text{DOPC}_{0.7}\text{DOPE}_{0.3}$ bilayer. The bending modulus increases in both the cases with the insertion of citral molecules, suggesting that the citral molecules make the membranes more rigid. The $\text{DOPC}_{0.7}\text{DOPE}_{0.3}$ bilayer showed an approx. 32% increase in κ , whereas the $\text{DOPC}_{0.7}\text{DOPG}_{0.3}$ bilayer exhibited an approx 11%

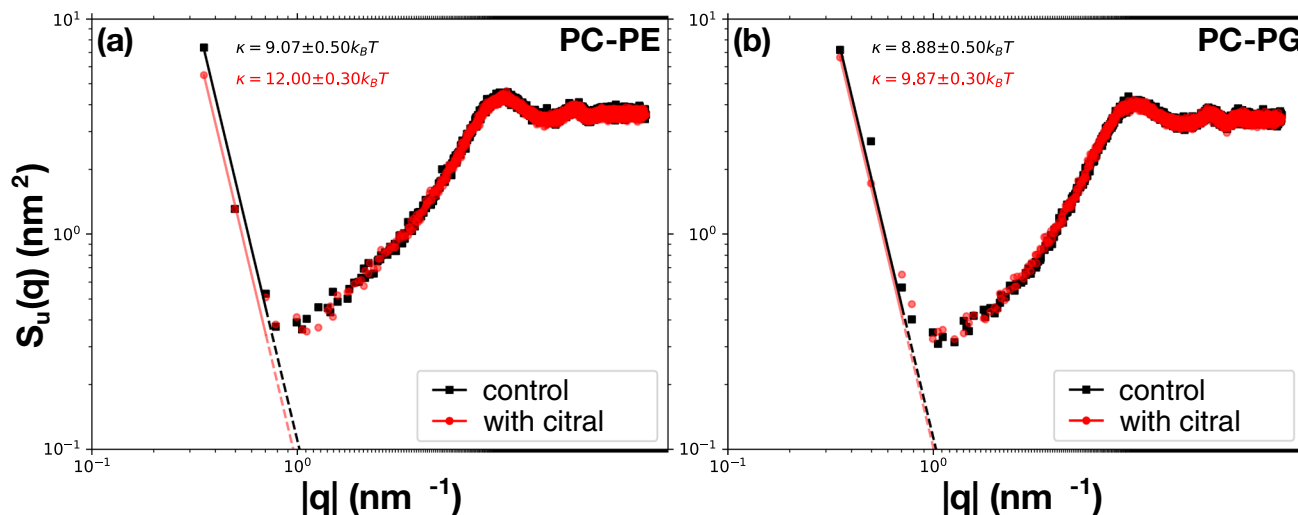


Fig. 4 Bending modulus for **a** $\text{DOPC}_{0.7}\text{DOPE}_{0.3}$ and **b** $\text{DOPC}_{0.7}\text{DOPG}_{0.3}$ lipid membranes, in presence and absence (control) of citral molecules. The solid lines represent the function fit on the data points obtained

increase. An increased bending modulus implies greater resistance to bending, resulting in reduced undulations. This resistance is higher in case of $\text{DOPC}_{0.7}\text{DOPE}_{0.3}$ bilayer, suggesting that it “stiffens” more compared to the $\text{DOPC}_{0.7}\text{DOPG}_{0.3}$ membrane that remains more flexible and deformable. Overall, the results suggest that citral molecules can have a significant effect on the bending mechanics of lipid bilayers.

3.5 Citral partitioning decreases lipid demixing and phase separation

Demixing in lipids, often referred to as phase separation or nano-domain formation in the membrane bilayer, involves the spatial segregation of lipid molecules into distinct regions or domains with differing lipid compositions and properties. This separation can arise from interactions between different lipid species or due to mechanistic effects of presence of other molecules. No persistent lipid nanodomains were observed within the timescales of the simulations. As a reporter of local lipid clustering and demixing, we calculated the Shannon entropy of mixing and probed the impact of citral molecules on the arrangement of different lipid species in the two membranes. The two lipids were considered and Shannon entropy of mixing was calculated between them, independent of the presence or absence of the citrals. We observed that the entropy was low, ranging between 0.2 and 0.3, compared to that of an ideal uniformly mixed system (0.69). Overall the $\text{DOPC}_{0.7}\text{DOPE}_{0.3}$ membrane system shows lower values of entropy than the $\text{DOPC}_{0.7}\text{DOPG}_{0.3}$ bilayer indicating higher demixing within the lipid species DOPC and DOPE. Both the membranes exhibited higher Shannon entropy, suggesting reduced demixing within the constituent lipid species in presence of citral molecules. However, further sampling is required due to the large dynamics in the membranes.

3.6 Citral cluster–membrane interaction

To increase the sampling and investigate the effect of the citral molecules on model membranes, we first considered the monomers in solution as the monomers partition into membranes relatively faster. However, citral molecules self-assemble in solvents and would exist as aggregates in experimental settings. To mimic the aggregation of citral molecules, we performed molecular dynamics simulations in aqueous solvent, based on our previous work [53]. We started with a set of randomly distributed citral molecules in water and simulated their interactions over time. The concentrations of citral molecules were varied between 1:555 and 1:75 (See Fig. S5). Overall, citral molecules have a strong tendency to self-assemble in aqueous solvent and the size and stability of the self-assemblies depend on the concentration of citral molecules. At low concentrations, citral molecules form dynamic aggregates with a tendency to fragment whereas at higher concentrations, citral molecules form larger, more stable aggregates. However, even at the lowest concentration, 80% molecules always comprise the main aggregate. The aggregation process is quantified by calculating the aggregation number of the self-assemblies at different concentrations which is presented in Fig. S5. As expected, the aggregation number was observed to decrease with increasing concentration.

We chose the smallest (1:555) and largest (1:75) aggregates to study their effects on the model bilayers under consideration. The interaction of the small cluster (consisting of 30 citral molecules) with $\text{DOPC}_{0.7}\text{DOPE}_{0.3}$ bilayer is depicted in Fig. 6 in a time-series representation. In the presence of the membrane the small cluster

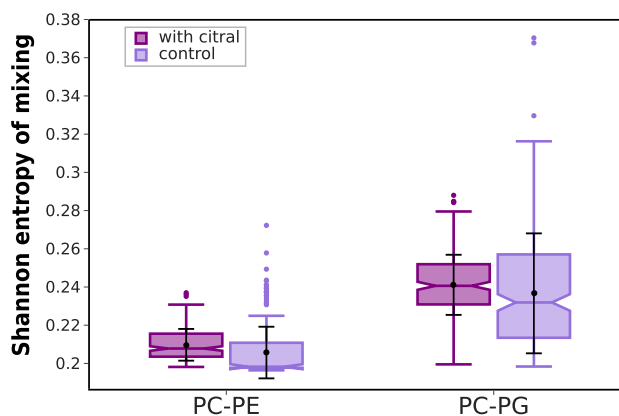


Fig. 5 Boxplots representing the variation in the values of Shannon entropy of mixing between the lipids for $\text{DOPC}_{0.7}\text{DOPE}_{0.3}$ and $\text{DOPC}_{0.7}\text{DOPG}_{0.3}$ lipid membranes, in presence and absence(control) of citral molecules calculated over the last 500 ns of the simulation trajectory. The data is averaged over three replicate simulation sets and the black solid lines represent the standard deviation values around the mean (represented by black dots)

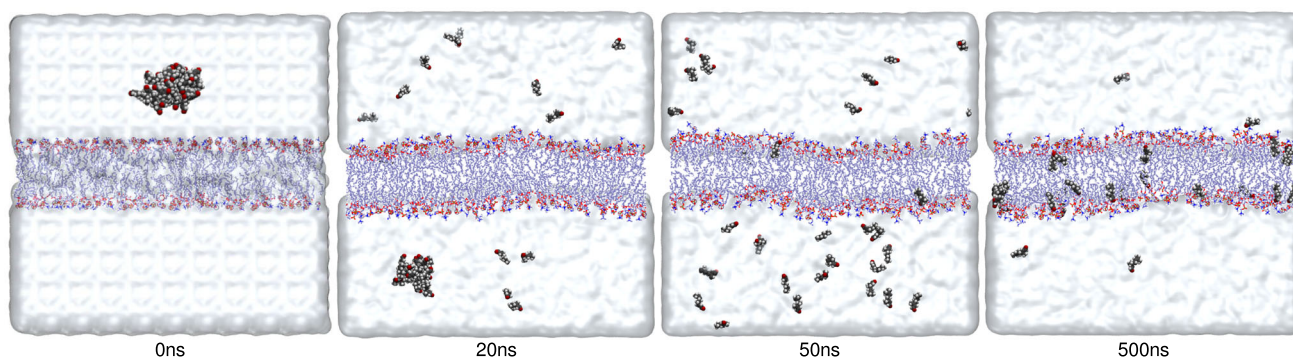


Fig. 6 A time series of representative snapshots of 30-molecule citral cluster interacting with $\text{DOPC}_{0.7}\text{-DOPE}_{0.3}$ membrane

slowly breaks down into monomers and these monomers then enter into the membrane in a similar manner as described in the previous sections. Within 50 ns, the entire cluster breaks down into individual molecules. Most of these monomers enter in the membrane within 500 ns and this permeation behavior is similar in both $\text{DOPC}_{0.7}\text{-DOPE}_{0.3}$ and $\text{DOPC}_{0.7}\text{-DOPG}_{0.3}$ systems. In case of the large cluster, the similar process occurs; the time required for the fragmentation of the cluster entirely is much longer than that of the small cluster (see Fig. S6). Surprisingly, in the absence of the membrane, the large cluster remains stable over microsecond timescale simulations. However, in the vicinity of the membrane, it starts to fragment and the individual citral monomers partition into the membrane as before.

4 Discussion

The interactions and subsequent effects of metabolites and xenobiotics on cell membranes is an important aspect of their cellular role and potential toxicity. In this study, we characterized the molecular-level interactions between citral monomers and spontaneously assembled clusters with $\text{DOPC}_{0.7}\text{-DOPE}_{0.3}$ and $\text{DOPC}_{0.7}\text{-DOPG}_{0.3}$ model membranes. Regardless of their initial aggregation state, citral molecules interacted with the membranes as monomers and mainly partitioned at the interface between the glycerol group and acyl chains. Notably, the presence of citral monomers modulated membrane fluidity by decreasing the order in acyl chain terminal carbons. Although the membrane interactions were similar across the two membrane systems, mechanical properties exhibited important differences. These findings underscore the nuanced impact of citral on membrane dynamics and structure, providing valuable insights into the molecular mechanisms underlying its interactions with distinct lipid compositions.

In the current work, significant alterations in membrane mechanics were observed upon citral partitioning and both fluidity and bending modulus were shown to be altered. We observed that the fluidity changes were not uniform and decreased at the interface whereas it increased toward the lipid termini. Overall, this led to a decrease

in the softness of the membrane. In general, it has been reported that bulk membrane viscosity and transverse membrane stiffness are often correlated, but co-dependent on other membrane properties, such as the lipid packing density, membrane permeability, and bending rigidity [68]. Despite extensive measurements of the bending moduli of various model membranes [69], comparative data on how small molecules like antibiotics or antimicrobials alter these values remain surprisingly limited. This limits our understanding of how such molecules influence membrane dynamics and potentially contribute to their effects on cellular processes. Recently, the epsin N-terminal homology (ENTH) protein domains were shown to result in a remarkable softening of POPC membranes upon protein binding, with bending moduli decreasing by about 32% and 47% depending on the protein-binding site [70]. This highlights the significant impact protein–lipid interactions can have on mechanical properties of membranes. Our work reveals a substantial stiffening of both DOPC:DOPE and DOPC:DOPG membranes due to citral partitioning. The bending moduli increased by 32% for DOPC:DOPE and 11% for DOPC:DOPG compared to the control membranes. Notably, this stiffening effect was comparable to the changes observed in studies examining protein-induced stiffening, despite the significantly smaller size of citral molecules. Furthermore, studies with saturated fatty dodecylamine or palmitic acid demonstrate that membrane stiffening can inhibit bacterial growth [71], suggesting a potential link between metabolite-induced stiffening and its antimicrobial activity. In contrast, the antibiotic, azithromycin has been shown to soften membranes [72, 73]. A more systematic comparison of the membrane effects of different antibiotics and antimicrobials is required to understand this complex effect.

Lipid nano/microdomains, ordered regions within the generally disordered membrane environment, have been extensively studied using various techniques [74–76]. Shannon entropy formalism is usually applied to study correlations in system exhibiting any kind of disorder–order phase transition, such as fluid mixtures and liquid crystals [77]. Other noteworthy methods include Voronoi edge lipid mixing entropy [78] and contact fraction analysis [79]. Further, the quantification of demixing through free energies offers an indirect yet insightful approach to understanding the thermodynamics of lipid demixing [80]. By considering Shannon entropy, we were able to discern a reduced nano-domain formation in both membranes, although the simple model membrane lacked the complexity of real membranes and large-scale phase separation. Similar studies using coarse-grained models suggest mixed effects of small molecules on lipid mixing, depending on their properties (aromaticity, hydrophobicity, polar nature etc.) and the membrane composition [79, 81]. Notably, azithromycin, an antibiotic, disrupts microdomains as well as softens membranes, potentially hindering bacterial attachment [72, 73]. Similarly, the importance of these domains for microbial defense mechanisms has been highlighted in studies considering the ceramide-1-phosphate molecule [82]. While directly comparing the current simulations with such studies is challenging due to timescale differences, our observations hint at an initial disruption of membrane organization by citral, potentially impacting domain dynamics. Further studies with longer simulations or alternative methodologies could provide more conclusive data on citral's long-term effects on nano/microdomains. While alterations in membrane rigidity or domain perturbation by metabolites are not always consistent predictors of antimicrobial activity, analyzing these properties in the citral–membrane simulations provides valuable insights into its potential antimicrobial effects, even without direct evidence of membrane integrity loss.

5 Conclusion

In summary, we performed all-atom classical molecular dynamics simulations to investigate the distinct effects of the plant metabolite—citral on model lipid bilayers composed of DOPC_{0.7}–DOPE_{0.3} and DOPC_{0.7}–DOPG_{0.3}, representing mammalian and bacterial cell membranes, respectively. Our simulations show that citral monomers readily partition into the membrane, with no discernible differences based on lipid composition. These monomers exhibited a preference for localizing near the acyl chains of the lipids, inducing changes in lipid fluidity, as evidenced by alterations in the acyl chain order parameter, thickness, and area per lipid. Furthermore, our findings indicated a notable impact of citral molecules on the rigidity of lipid bilayers, with a significantly higher bending modulus observed in the DOPC_{0.7}–DOPE_{0.3} lipid bilayers compared to the DOPC_{0.7}–DOPG_{0.3} bilayers. The DOPC_{0.7}–DOPE_{0.3} membrane system exhibited a greater propensity for demixing among its constituent lipid species, as indicated by Shannon entropy calculations, compared to the DOPC_{0.7}–DOPG_{0.3} bilayer. Additionally, the simulations of the citral aggregates interacting with membranes revealed a fragmentation of the aggregates into monomers, ultimately leading to their partitioning into the membrane. These results contribute to a comprehensive understanding of the intricate interactions between citral and lipid bilayers, shedding light on the potential implications for cellular membranes and offering insights that may guide future drug development and delivery strategies.

Supplementary Information The online version contains supplementary material available at <https://doi.org/10.1140/epjs/s11734-024-01147-w>.

Acknowledgements Deepashri Saraf and Sudha Porte would like to acknowledge CSIR (India) for financial support through research associate fellowship and junior research fellowship, respectively. D.S. acknowledges the support of the Bioinformatics center from DBT, India (BT/PR40128/BTIS/137/43/2022) hosted at CSIR-NCL, India. We gratefully acknowledge computing resources from CSIR-NCL, CSIR-Fourth Paradigm Institute and PARAM Brahma Facility under the National Supercomputing Mission, Government of India at the Indian Institute of Science Education and Research (IISER) Pune. Deepashri would like to thank Amit Naglekar and Siddhanta Nikte for the insightful discussions on analysis tools and image rendering. We thank Prof. Ganapathy Ayappa and Prof. Anand Srivastava for helpful discussions. The authors would like to thank our research group members for critically reading the manuscript.

Author contribution statement

Deepashri Saraf: data curation, formal analysis, investigation, methodology, software, writing—original draft preparation. Sudha Porte: formal analysis, investigation, methodology, writing—review and editing. Durba Sengupta: conceptualization, funding acquisition, project administration, resources, supervision, validation, writing—review and editing.

Funding Bioinformatic center, DBT-India (BT/PR40128/BTIS/137/43/2022).

Data availability statement This manuscript has data included as electronic supplementary material.

Declarations

Conflict of interest The authors have no conflicts to disclose.

Ethics approval Not applicable.

Consent to participate Not applicable.

Consent for publication Not applicable.

Code availability Not applicable.

References

1. G.L. Nicolson, G.F. Mattos, The fluid-mosaic model of cell membranes: a brief introduction, historical features, some general principles, and its adaptation to current information. *Biochim. Biophys. Acta-Biomembr.* **1865**(4), 184135 (2023). <https://doi.org/10.1016/j.bbamem.2023.184135>
2. P.V. Escribá, J.M. González-Ros, F.M. Goñi, P.K. Kinnunen, L. Vigh, L. Sánchez-Magraner, A.M. Fernández, X. Busquets, I. Horváth, G. Barceló-Coblijn, Membranes: A meeting point for lipids, proteins and therapies. *J. Cell. Mol. Med.* **12**(3), 829–875 (2008). <https://doi.org/10.1111/j.1582-4934.2008.00281.x>
3. I. Budin, J.W. Szostak, Expanding roles for diverse physical phenomena during the origin of life. *Annu. Rev. Biophys.* **39**, 245–263 (2010). <https://doi.org/10.1146/annurev.biophys.050708.133753>
4. J.L. Robertson, The lipid bilayer membrane and its protein constituents. *J. Gen. Physiol.* **150**(11), 1472–1483 (2018). <https://doi.org/10.1085/jgp.201812153>
5. G. Meer, A.I. Kroon, Lipid map of the mammalian cell. *J. Cell Sci.* **124**(1), 5–8 (2011). <https://doi.org/10.1242/jcs.071233>
6. I. Levental, K.R. Levental, F.A. Heberle, Lipid rafts: Controversies resolved, mysteries remain. *Trends Cell Biol.* **30**(5), 341–353 (2020). <https://doi.org/10.1016/j.tcb.2020.01.009>
7. D. Lingwood, K. Simons, Lipid rafts as a membrane-organizing principle. *Science* **327**(5961), 46–50 (2010). <https://doi.org/10.1126/science.1174621>
8. S. Haldar, M. Kombrabail, G. Krishnamoorthy, A. Chattopadhyay, Depth-dependent heterogeneity in membranes by fluorescence lifetime distribution analysis. *J. Phys. Chem. Lett.* **3**(18), 2676–2681 (2012). <https://doi.org/10.1021/jz3012589>
9. J.F. Nagle, S. Tristram-Nagle, Structure of lipid bilayers. *Biochim. Biophys. Acta.* **1469**(3), 159–195 (2000). [https://doi.org/10.1016/s0304-4157\(00\)00016-2](https://doi.org/10.1016/s0304-4157(00)00016-2)
10. O.S. Ollila, G. Pabst, Atomistic resolution structure and dynamics of lipid bilayers in simulations and experiments. *Biochim. Biophys. Acta-Biomembr.* **1858**(10), 2512–2528 (2016). <https://doi.org/10.1016/j.bbamem.2016.01.019>
11. G. Van Meer, D.R. Voelker, G.W. Feigenson, Membrane lipids: Where they are and how they behave. *Nat. Rev. Mol. Cell Biol.* **9**(2), 112–124 (2008). <https://doi.org/10.1038/nrm2330>
12. T. Harayama, H. Riezman, Understanding the diversity of membrane lipid composition. *Nat. Rev. Mol. Cell Biol.* **19**(5), 281–296 (2018). <https://doi.org/10.1038/nrm.2017.138>

13. K. Jacobson, O.G. Mouritsen, R.G. Anderson, Lipid rafts: At a crossroad between cell biology and physics. *Nat. Cell Biol.* **9**(1), 7–14 (2007). <https://doi.org/10.1038/ncb0107-7>
14. R. Friedman, S. Khalid, C. Aponte-Santamaría, E. Arutyunova, M. Becker, K.J. Boyd, M. Christensen, J.T. Coimbra, S. Concilio, C. Daday et al., Understanding conformational dynamics of complex lipid mixtures relevant to biology. *J. Membr. Biol.* **251**, 609–631 (2018). <https://doi.org/10.1007/s00232-018-0050-y>
15. E. Sezgin, I. Levental, S. Mayor, C. Eggeling, The mystery of membrane organization: composition, regulation and roles of lipid rafts. *Nat. Rev. Mol. Cell Biol.* **18**(6), 361–374 (2017). <https://doi.org/10.1038/nrm.2017.16>
16. P. Bassereau, R. Jin, T. Baumgart, M. Deserno, R. Dimova, V.A. Frolov, P.V. Bashkirov, H. Grubmüller, R. Jahn, H.J. Risselada et al., The 2018 biomembrane curvature and remodeling roadmap. *J. Phys. D: Appl. Phys.* **51**(34), 343001 (2018). <https://doi.org/10.1088/1361-6463/aacb98>
17. J.L. MacCallum, D.P. Tieleman, in *Current Topics in Membranes. Interactions Between Small Molecules and Lipid Bilayers*, vol. 60 (Elsevier, New York, 2008), pp. 227–256. [https://doi.org/10.1016/S1063-5823\(08\)00008-2](https://doi.org/10.1016/S1063-5823(08)00008-2)
18. N.J. Yang, M.J. Hinner, Getting across the cell membrane: an overview for small molecules, peptides, and proteins. *Met. Mol. Biol.* (2014). https://doi.org/10.1007/978-1-4939-2272-7_3
19. C. Martinotti, L. Ruiz-Perez, E. Deplazes, R.L. Mancera, Molecular dynamics simulation of small molecules interacting with biological membranes. *ChemPhysChem* **21**(14), 1486–1514 (2020). <https://doi.org/10.1002/cphc.202000219>
20. J. Frallicciardi, J. Melcr, P. Siginou, S.J. Marrink, B. Poolman, Membrane thickness, lipid phase and sterol type are determining factors in the permeability of membranes to small solutes. *Nat. Commun.* (2022). <https://doi.org/10.1038/s41467-022-29272-x>
21. D. Sengupta, J.C. Smith, G.M. Ullmann, Partitioning of amino-acid analogues in a five-slab membrane model. *Biochim. Biophys. Acta-Biomembr.* **1778**(10), 2234–2243 (2008). <https://doi.org/10.1016/j.bbamem.2008.06.014>
22. M. Orsi, W.E. Sanderson, J.W. Essex, Permeability of small molecules through a lipid bilayer: A multiscale simulation study. *J. Phys. Chem. B* **113**(35), 12019–12029 (2009). <https://doi.org/10.1021/jp903248s>
23. B.M. Schmidt, D.M. Ribnicky, P.E. Lipsky, I. Raskin, Revisiting the ancient concept of botanical therapeutics. *Nat. Chem. Biol.* **3**(7), 360–366 (2007). <https://doi.org/10.1038/nchembio0707-360>
24. D.C. Arruda, D.C. Miguel, J.K.U. Yokoyama-Yasunaka, A.M. Katzin, S.R.B. Uliana, Inhibitory activity of limonene against leishmania parasites in vitro and in vivo. *Biomed. Pharmacother.* **63**(9), 643–649 (2009). <https://doi.org/10.1016/j.biopha.2009.02.004>
25. Wu, C.-S., Chen, Y.-J., Chen, J.J.W., Shieh, J.-J., Huang, C.-H., Lin, P.-S., Chang, G.-C., Chang, J.-T., Lin, C.-C.: Terpinen-4-ol induces apoptosis in human nonsmall cell lung cancer in vitro and in vivo. In: eCAM 2012, 1–13 (2012) <https://doi.org/10.1155/2012/818261>
26. H. Yang, Q. Ping Dou, Targeting apoptosis pathway with natural terpenoids: Implications for treatment of breast and prostate cancer. *Curr. Drug Targets* **11**(6), 733–744 (2010). <https://doi.org/10.2174/138945010791170842>
27. M.E. Araruna, C. Serafim, E.A. Júnior, C. Hiruma-Lima, M. Diniz, L. Batista, Intestinal anti-inflammatory activity of terpenes in experimental models (2010–2020): A review. *Molecules* **25**(22), 5430 (2020). <https://doi.org/10.3390/molecules25225430>
28. S.A. Mendanha, A. Alonso, Effects of terpenes on fluidity and lipid extraction in phospholipid membranes. *Biophys. Chem.* **198**, 45–54 (2015). <https://doi.org/10.1016/j.bpc.2015.02.001>
29. A. Zielńska, C. Martins-Gomes, N.R. Ferreira, A.M. Silva, I. Nowak, E.B. Souto, Anti-inflammatory and anti-cancer activity of citral: optimization of citral-loaded solid lipid nanoparticles (SLN) using experimental factorial design and LUMiSizer®. *Int. J. Pharm.* **553**(1–2), 428–440 (2018). <https://doi.org/10.1016/j.ijpharm.2018.10.065>
30. C. Bailly, Targets and pathways involved in the antitumor activity of citral and its stereo-isomers. *Eur. J. Pharmacol.* **871**, 172945 (2020). <https://doi.org/10.1016/j.ejphar.2020.172945>
31. N. Nordin, S.K. Yeap, H.S. Rahman, N.R. Zambari, N.E. Mohamad, N. Abu, M.J. Masarudin, R. Abdullah, N.B. Alitheen, Antitumor and anti-metastatic effects of citral-loaded nanostructured lipid carrier in 4t1-induced breast cancer mouse model. *Molecules* **25**(11), 2670 (2020). <https://doi.org/10.3390/molecules25112670>
32. S.A. Singh, Y.A. Potdar, R.S. Pawar, S.V. Bhat, Antibacterial potential of citral derivatives. *Nat. Prod. Commun.* **6**(9), 1221–1224 (2011)
33. A. Tetard, S. Foley, G.L.A. Mislin, J.-M. Brunel, E. Oliva, F.T. Anzola, A. Zedet, B. Cardey, Y. Pellequer, C. Ramseyer, P. Plésiat, C. Llanes, Negative impact of citral on susceptibility of *Pseudomonas aeruginosa* to antibiotics. *Front. Microbiol.* (2021). <https://doi.org/10.3389/fmicb.2021.709838>
34. R.-Y. Li, X.-M. Wu, X.-H. Yin, Y.-H. Long, M. Li, Naturally produced citral can significantly inhibit normal physiology and induce cytotoxicity on *Magnaporthe grisea*. *Pestic. Biochem. Physiol.* **118**, 19–25 (2015). <https://doi.org/10.1016/j.pestbp.2014.10.015>
35. G. Shahane, W. Ding, M. Palaiokostas, M. Orsi, Physical properties of model biological lipid bilayers: insights from all-atom molecular dynamics simulations. *J. Mol. Model.* (2019). <https://doi.org/10.1007/s00894-019-3964-0>
36. R.M. Venable, A. Krämer, R.W. Pastor, Molecular dynamics simulations of membrane permeability. *Chem. Rev.* **119**(9), 5954–5997 (2019). <https://doi.org/10.1021/acs.chemrev.8b00486>
37. W.J. Allen, J.A. Lemkul, D.R. Bevan, GridMAT-MD: a grid-based membrane analysis tool for use with molecular dynamics. *J. Comput. Chem.* **30**(12), 1952–1958 (2008). <https://doi.org/10.1002/jcc.21172>
38. M. Chavent, T. Reddy, J. Goose, A.C.E. Dahl, J.E. Stone, B. Jobard, M.S.P. Sansom, Methodologies for the analysis of instantaneous lipid diffusion in md simulations of large membrane systems. *Faraday Discuss.* **169**, 455–475 (2014). <https://doi.org/10.1039/c3fd00145h>

39. G. Lukat, J. Krüger, B. Sommer, APL@Voro: a voronoi-based membrane analysis tool for GROMACS trajectories. *J. Chem. Inf. Model.* **53**(11), 2908–2925 (2013). <https://doi.org/10.1021/ci400172g>
40. H. Hoppe, T. DeRose, T. Duchamp, J. McDonald, W. Stuetzle, Surface reconstruction from unorganized points. *ACM SIGGRAPH Comput. Graph.* **26**(2), 71–78 (1992). <https://doi.org/10.1145/142920.134011>
41. R. Guixà-González, I. Rodríguez-Espigares, J.M. Ramírez-Anguita, P. Carrió-Gaspar, H. Martínez-Seara, T. Giorgino, J. Selent, MEMBPLUGIN: studying membrane complexity in VMD. *Bioinformatics* **30**(10), 1478–1480 (2014). <https://doi.org/10.1093/bioinformatics/btu037>
42. H. Malshikare, S. Prakash, D. Sengupta, Differential membrane curvature induced by distinct protein conformers *Soft Matter* **19**(22), 4021–4028 (2023). <https://doi.org/10.1039/D3SM00218G>
43. S.J. Marrink, V. Corradi, P.C.T. Souza, H.I. Ingólfsson, D.P. Tieleman, M.S.P. Sansom, Computational modeling of realistic cell membranes. *Chem. Rev.* **119**(9), 6184–6226 (2019). <https://doi.org/10.1021/acs.chemrev.8b00460>
44. R. Wadhwa, N.S. Yadav, S.P. Katiyar, T. Yaguchi, C. Lee, H. Ahn, C.-O. Yun, S.C. Kaul, D. Sundar, Molecular dynamics simulations and experimental studies reveal differential permeability of withaferin-A and withanone across the model cell membrane. *Sci. Rep.* **11**, 2352 (2021). <https://doi.org/10.1038/s41598-021-81729-z>
45. B. Van Oosten, D. Marquardt, I. Komljenović, J.P. Bradshaw, E. Sternin, T.A. Harroun, Small molecule interaction with lipid bilayers: a molecular dynamics study of chlorhexidine. *J. Mol. Graph. Model.* **48**, 96–104 (2014). <https://doi.org/10.1016/j.jmgm.2013.12.007>
46. T. Jin, S.J. Patel, R.C. Van Lehn, Molecular simulations of lipid membrane partitioning and translocation by bacterial quorum sensing modulators. *PLoS One* **16**(2), 0246187 (2021). <https://doi.org/10.1371/journal.pone.0246187>
47. Q.P. Pham, D. Topgaard, E. Sparr, Cyclic and linear monoterpenes in phospholipid membranes: phase behavior, bilayer structure, and molecular dynamics. *Langmuir* **31**(40), 11067–11077 (2015). <https://doi.org/10.1021/acs.langmuir.5b00856>
48. S. Raza, M. Miller, B. Hamberger, J.V. Vermaas, Plant terpenoid permeability through biological membranes explored via molecular simulations. *J. Phys. Chem. B* **127**(5), 1144–1157 (2023). <https://doi.org/10.1021/acs.jpccb.2c07209>
49. P. Bjelkmar, P. Larsson, M.A. Cuendet, B. Hess, E. Lindahl, Implementation of the CHARMM force field in GROMACS: analysis of protein stability effects from correction maps, virtual interaction sites, and water models. *J. Chem. Theory Comput.* **6**, 459–466 (2010). <https://doi.org/10.1021/ct900549r>
50. B. Hess, C. Kutzner, D. Spoel, E. Lindahl, Algorithms for highly efficient, load-balanced, and scalable molecular simulation. *J. Chem. Theory Comput.* **4**, 435–447 (2008). <https://doi.org/10.1021/ct700301q>
51. K. Vanommeslaeghe, E. Hatcher, C. Acharya, S. Kundu, S. Zhong, J. Shim, E. Darian, O. Guvench, P. Lopes, I. Vorobyov, A.D. MacKerell Jr., CHARMM General Force Field (CGenFF): a force field for drug-like molecules compatible with the CHARMM all-atom additive biological force fields. *J. Comput. Chem.* **31**(4), 671–690 (2010). <https://doi.org/10.1002/jcc.21367>
52. W. Yu, X. He, K. Vanommeslaeghe, A.D. MacKerell Jr., Extension of the CHARMM General Force Field to sulfonyl-containing compounds and its utility in biomolecular simulations. *J. Comput. Chem.* **33**(31), 2451–2468 (2012). <https://doi.org/10.1002/jcc.23067>
53. D. Saraf, S. Prakash, A. Pinjari, B. Pujari, D. Sengupta, Surface-induced demixing of self-assembled isomeric mixtures of citral. *J. Mol. Liq.* **381**, 121803 (2023). <https://doi.org/10.1016/j.molliq.2023.121803>
54. B.R. Brooks, R.E. Bruccoleri, B.D. Olafson, D.J. States, S. Swaminathan, M. Karplus, CHARMM: a program for macromolecular energy, minimization, and dynamics calculations. *J. Comput. Chem.* **4**, 187–217 (1983). <https://doi.org/10.1002/jcc.540040211>
55. W.L. Jorgensen, J. Chandrasekhar, J.D. Madura, R.W. Impey, M.L. Klein, Comparison of simple potential functions for simulating liquid water. *J. Chem. Phys.* **79**, 926–935 (1983). <https://doi.org/10.1063/1.445869>
56. H.J.C. Berendsen, J.P.M. Postma, W.F. Gunsteren, A. DiNola, J.R. Haak, Molecular dynamics with coupling to an external bath. *J. Chem. Phys.* **81**, 3684–3690 (1984). <https://doi.org/10.1063/1.448118>
57. H.J.C. Berendsen, D. Spoel, R. Drunen, GROMACS: A message-passing parallel molecular dynamics implementation. *Comp. Phys. Comm.* **91**, 43–56 (1995). [https://doi.org/10.1016/0010-4655\(95\)00042-E](https://doi.org/10.1016/0010-4655(95)00042-E)
58. M. Parinello, A. Rahman, Polymorphic transitions in single crystals: a new molecular dynamics method. *J. Appl. Phys.* **52**, 7182 (1981). <https://doi.org/10.1063/1.328693>
59. B. Hess, H. Bekker, H.J.C. Berendsen, J.G.E.M. Fraaije, LINCS: a linear constraint solver for molecular simulations. *J. Comput. Chem.* **18**, 1463–1472 (1997). <https://doi.org/10.1063/1.3382344>
60. W. Humphrey, A. Dalke, K. Schulten, VMD-visual molecular dynamics. *J. Mol. Graph.* **14**, 33–38 (1996). [https://doi.org/10.1016/0263-7855\(96\)00018-5](https://doi.org/10.1016/0263-7855(96)00018-5)
61. S. Buchoux, FATSLiM: a fast and robust software to analyze MD simulations of membranes. *Bioinformatics* **33**(1), 133–134 (2016). <https://doi.org/10.1093/bioinformatics/btw563>
62. M. Camesasca, M. Kaufman, I. Manas-Zloczower, Quantifying fluid mixing with the shannon entropy. *Macromol. Theory Simul.* **15**, 595–607 (2006). <https://doi.org/10.1002/mats.200600037>
63. W. Helfrich, Elastic properties of lipid bilayers: theory and possible experiments. *Z. Naturforsch. C* **28**, 693–703 (1973)
64. F.M. Thakkar, P.K. Maiti, V. Kumaran, K.G. Ayappa, Verifying scalings for bending rigidity of bilayer membranes using mesoscale models. *Soft Matter* **7**(8), 3963 (2011). <https://doi.org/10.1039/c0sm00876a>
65. R. Vaiwala, P. Sharma, M. Puranik, K.G. Ayappa, Developing a coarse-grained model for bacterial cell walls: evaluating mechanical properties and free energy barriers. *J. Chem. Theory Comput.* **16**(8), 5369–5384 (2020). <https://doi.org/10.1021/acs.jctc.0c00539>

66. V. Zoni, P. Campomanes, S. Vanni, Investigating the structural properties of hydrophobic solvent-rich lipid bilayers. *Soft Matter* **17**(21), 5329–5335 (2021). <https://doi.org/10.1039/d0sm02270e>
67. G. Abbas, A.E. Cardenas, R. Elber, The structures of heterogeneous membranes and their interactions with an anticancer peptide: a molecular dynamics study. *Life* **12**(10), 1473 (2022). <https://doi.org/10.3390/life12101473>
68. M.F. Renne, R. Ernst, Membrane homeostasis beyond fluidity: control of membrane compressibility. *Trends Biochem. Sci.* **48**, 963–977 (2023). <https://doi.org/10.1016/j.tibs.2023.08.004>
69. D. Bochicchio, L. Monticelli, *The Membrane Bending Modulus in Experiments and Simulations* (Elsevier, 2016), pp.117–143. <https://doi.org/10.1016/bs.abl.2016.01.003>
70. T. Mandal, S. Gupta, J. Soni, Simulation study of membrane bending by protein crowding: a case study with the epsin n-terminal homology domain. *Soft Matter* **19**(27), 5092–5102 (2023). <https://doi.org/10.1039/d3sm00280b>
71. S. Salinas-Almaguer, M. Mell, V.G. Almendro-Vedia, M. Calero, K.C.M. Robledo-Sánchez, C. Ruiz-Suarez, T. Alarcón, R.A. Barrio, A. Hernández-Machado, F. Monroy, Membrane rigidity regulates *E. coli* proliferation rates. *Sci. Rep.* (2022). <https://doi.org/10.1038/s41598-022-04970-0>
72. A. Berquand, M.-P. Mingeot-Leclercq, Y.F. Dufrêne, Real-time imaging of drug-membrane interactions by atomic force microscopy. *Biochim. Biophys. Acta Biomembr.* **1664**(2), 198–205 (2004). <https://doi.org/10.1016/j.bbamem.2004.05.010>
73. N. Fa, L. Lins, P.J. Courtoy, Y. Dufrêne, P. Van Der Smissen, R. Brasseur, D. Tyteca, M.-P. Mingeot-Leclercq, Decrease of elastic moduli of dopc bilayers induced by a macrolide antibiotic, azithromycin. *Biochim. Biophys. Acta Biomembr.* **1768**(7), 1830–1838 (2007). <https://doi.org/10.1016/j.bbamem.2007.04.013>
74. L.J. Pike, The challenge of lipid rafts. *J. Lipid Res.* **50**, 323–328 (2009). <https://doi.org/10.1194/jlr.r800040-jlr200>
75. G.W. Feigenson, Phase diagrams and lipid domains in multicomponent lipid bilayer mixtures. *Biochim. Biophys. Acta Biomembr.* **1788**(1), 47–52 (2009). <https://doi.org/10.1016/j.bbamem.2008.08.014>
76. J. Fan, M. Sammalkorpi, M. Haataja, Formation and regulation of lipid microdomains in cell membranes: theory, modeling, and speculation. *FEBS Lett.* **584**(9), 1678–1684 (2009). <https://doi.org/10.1016/j.febslet.2009.10.051>
77. G.B. Brandani, M. Schor, C.E. MacPhee, H. Grubmüller, U. Zachariae, D. Marenduzzo, Quantifying disorder through conditional entropy: an application to fluid mixing. *PLoS One* **8**(6), 65617 (2013). <https://doi.org/10.1371/journal.pone.0065617>
78. G.A. Pantelopulos, T. Nagai, A. Bandara, A. Panahi, J.E. Straub, Critical size dependence of domain formation observed in coarse-grained simulations of bilayers composed of ternary lipid mixtures. *J. Chem. Phys.* (2017). <https://doi.org/10.1063/1.4999709>
79. J. Barnoud, G. Rossi, S.J. Marrink, L. Monticelli, Hydrophobic compounds reshape membrane domains. *PLoS Comput. Biol.* **10**(10), 1003873 (2014). <https://doi.org/10.1371/journal.pcbi.1003873>
80. W.F.D. Bennett, J.-E. Shea, D.P. Tieleman, Phospholipid chain interactions with cholesterol drive domain formation in lipid membranes. *Biophys. J.* **114**(11), 2595–2605 (2018). <https://doi.org/10.1016/j.bpj.2018.04.022>
81. A. Centi, A. Dutta, S.H. Parekh, T. Bereau, Inserting small molecules across membrane mixtures: Insight from the potential of mean force. *Biophys. J.* **118**(6), 1321–1332 (2020). <https://doi.org/10.1016/j.bpj.2020.01.039>
82. D. Drabik, M. Drab, S. Penič, A. Iglíč, A. Czogalla, Investigation of nano- and microdomains formed by ceramide 1 phosphate in lipid bilayers. *Sci. Rep.* (2023). <https://doi.org/10.1038/s41598-023-45575-5>

Springer Nature or its licensor (e.g. a society or other partner) holds exclusive rights to this article under a publishing agreement with the author(s) or other rightsholder(s); author self-archiving of the accepted manuscript version of this article is solely governed by the terms of such publishing agreement and applicable law.